

Single-Pion Production in pp Collisions at 0.95 GeV/c (II)

S. Abd El-Samad⁸, R. Bilger⁶, K.-Th. Brinkmann², H. Clement⁶, M. Dietrich⁶, E. Doroshkevich⁶, S. Dshemuchadse^{5,2}, K. Ehrhardt⁶, A. Erhardt⁶, W. Eyrich³, A. Filippi⁷, H. Freiesleben², M. Fritsch^{3,1}, R. Geyer⁴, A. Gillitzer⁴, J. Hauße³, D. Hesselbarth⁴, R. Jaekel², B. Jakob², L. Karsch², K. Kilian⁴, J. Kress⁶, E. Kuhlmann², S. Marcello⁷, S. Marwinski⁴, R. Meier⁶, K. Möller⁵, H.P. Morsch⁴, L. Naumann⁵, J. Ritman⁴, E. Roderburg⁴, P. Schönmeier^{2,3}, M. Schulte-Wissermann², W. Schroeder³, F. Stinzinger³, G.Y. Sun², J. Wächter³, G.J. Wagner⁶, M. Wagner³, U. Weidlich⁶, A. Wilms¹, S. Wirth³, G. Zhang^{6a}, and P. Zupranski⁹

¹ Ruhr-Universität Bochum, Germany

² Technische Universität Dresden, Germany

³ Friedrich-Alexander-Universität Erlangen-Nürnberg, Germany

⁴ Forschungszentrum Jülich, Germany

⁵ Forschungszentrum Rossendorf, Germany

⁶ Physikalisches Institut der Universität Tübingen, Tübingen, Germany

⁷ University of Torino and INFN, Sezione di Torino, Italy

⁸ Atomic Energy Authority NRC Cairo, Egypt

⁹ Soltan Institute for Nuclear Studies, Warsaw, Poland
(COSY-TOF Collaboration)

February 6, 2020

Abstract. The single-pion production reactions $pp \rightarrow d\pi^+$, $pp \rightarrow np\pi^+$ and $pp \rightarrow pp\pi^0$ were measured at a beam momentum of 0.95 GeV/c ($T_p \approx 400$ MeV) using the short version of the COSY-TOF spectrometer. The central calorimeter provided particle identification, energy determination and neutron detection in addition to time-of-flight and angle measurements from other detector parts. Thus all pion production channels were recorded with 1-4 overconstraints. Main emphasis is put on the presentation and discussion of the $np\pi^+$ channel, since the results on the other channels have already been published previously. The total and differential cross sections obtained are compared to theoretical calculations. In contrast to the $pp\pi^0$ channel we find in the $np\pi^+$ channel a strong influence of the Δ excitation already at this energy close to threshold. In particular we find a $(3 \cos^2\Theta + 1)$ dependence in the pion angular distribution, typical for a pure s-channel Δ excitation and identical to that observed in the $d\pi^+$ channel. Since the latter is understood by a s-channel resonance in the 1D_2 pn partial wave, we discuss an analogous scenario for the $pn\pi^+$ channel.

PACS. 13.75.Cs – 14.20.Gk – 14.20.Pt – 25.10.+s – 25.40.Ep

1 Introduction

Single-pion production in the collision between two nucleons is thought to be the simplest inelastic process between two baryons, nevertheless its understanding is still far from being satisfactory - both from the theoretical and the experimental point of view. In a recent publication [1] – in the following denoted by (I) – we have presented the first kinematically complete measurement for the $pp \rightarrow pp\pi^0$ channel at a beam momentum of 0.95 GeV/c (corresponding to $T_p = 397$ MeV). Although Δ production in relative s-wave is prohibited in this reaction channel, we have seen that the angular distributions indicate the presence of sig-

nificant Δ production in relative p-wave already close to threshold.

In this work we present our results for the $pp \rightarrow pn\pi^+$ channel at the same incident energy. We will show that here, where Δ production in relative s-wave is allowed, indeed this production process is overwhelmingly dominant and characterizes the differential observables in this channel.

2 Experiment

Since the experimental setup has been discussed in detail in (I), we give here only a short review. The measurements have been carried out at the Jülich Cooler Synchrotron COSY using the time-of-flight spectrometer TOF at one

^a present address: Peking University
Correspondence to: H. Clement
email: clement@pit.physik.uni-tuebingen.de

of its external beam lines. At the entrance of the detector system the beam - collimated to a diameter smaller than 2 mm - hits the LH₂ target, which has a length of 4 mm, a diameter of 6 mm and 0.9 μm thick hostaphan foils as entrance and exit windows. At a distance of 22 mm downstream of the target the two layers of the start detector (each consisting of 1 mm thick scintillators cut into 12 wedge-shaped sectors) were placed followed by a two-plane fiber hodoscope (96 x 96 fibers, 2 mm thick each) at a distance of 165 mm from target. Whereas the start detector mainly supplies the start time signals for the time-of-flight (TOF) measurements, the fiber hodoscope primarily provides a good angular resolution for the detected particle tracks. In its central part the TOF-stop detector system consists of the so-called Quirl, a 3-layer scintillator system 1081 mm downstream of the target – and in its peripheral part of the so-called Ring, also a 3-layer scintillator system built in a design analogous to the Quirl, however, with inner and outer radii of 560 and 1540 mm, respectively. Finally behind the Quirl a calorimeter was installed for identification of charged particles and of neutrons as well as for measuring the energy of charged particles. The calorimeter consists of 84 hexagon-shaped scintillator blocks of length 450 mm, which suffices to stop deuterons, protons and pions of energies up to 400, 300 and 160 MeV, respectively. The energy calibration of the calorimeter was performed by detecting cosmic muons.

In the experiment the trigger required two hits in Quirl and/or Ring associated with two hits in the start detector. Tracks of charged particles are reconstructed from straight-line fits to the hit detector elements. They are accepted as good tracks, if they originate in the target and have a hit in each detector element the track passes through. In this way the angular resolution is better than 1° both in azimuthal and in polar angles. If there is an isolated hit in the calorimeter with no associated hits in the preceding detector elements, then this hit qualifies as a neutron candidate (further criteria will be discussed below). In this case the angular resolution of the neutron track is given by the size of the hit calorimeter block, i.e. by 7 - 8°. By construction of the calorimeter a particle will hit one or more calorimeter blocks. The number of blocks hit by a particular particle is given by the track reconstruction. The total energy deposited by this particle in the calorimeter is then just the (calibrated) sum of energies deposited in all blocks belonging to the particular track.

In order to have maximum angular coverage by the detector elements and to minimize the fraction of charged pions decaying in flight before reaching the stop detectors, the short version of the TOF spectrometer was used. In this way a total polar angle coverage of $3^\circ \leq \Theta^{lab} \leq 49^\circ$ was achieved with the central calorimeter covering the region $3^\circ \leq \Theta^{lab} \leq 28^\circ$. For fast particles the energy resolution of the calorimeter amounting to 4% is superior to that from time-of-flight measurements due to the short path length. However, the time-of-flight resolution is still much better than the ΔE resolution of the Quirl elements. Hence, for particle identification, instead of plotting ΔE

versus E_{cal} , the uncorrected particle energy deposited in the calorimeter, we utilize the relation $\Delta E \sim (z/\beta)^2$ with the particle charge $z = 1$ and plot $1/\beta^2$ versus E_{cal} , where the particle velocity $\beta = v/c$ is derived from the time-of-flight measurement.

By identifying and reconstructing the two charged tracks of an event the exit channels $d\pi^+$, $np\pi^+$ and $pp\pi^0$ can be separated. Kinematically the maximum possible laboratory (lab) polar angles are $\approx 9^\circ$ for deuterons and $\approx 32^\circ$ for protons (and neutrons). Hence 86% of the angular coverage for protons and neutrons from single pion production are within the angular acceptance of the calorimeter. For charged pions the angular coverage has been much lower with this setup, since kinematically they can extend up to $\Theta^{lab} = 180^\circ$. Hence within the angular coverage of Quirl and Ring the angular acceptance for π^+ has been $\approx 40\%$ only. Nevertheless most of the phase space part necessary for a full coverage of the physics in single pion production has been covered (see below) by these measurements due to the circumstance that the center-of-mass (cm) angular distributions have to be symmetric about 90° because of identical collision partners in the incident channel.

The $np\pi^+$ channel is selected by identifying proton and pion in the calorimeter or only the proton in the calorimeter, when the second charged track is in the Ring. In addition, the missing $p\pi$ mass $MM_{p\pi}$ has to meet the condition $900 \text{ MeV}/c^2 \leq MM_{p\pi} \leq 980 \text{ MeV}/c^2$. Also to suppress background from the $d\pi^+$ channel - in particular when the deuteron breaks up and appears as a proton in the calorimeter - the $p\pi^+$ track is required to be non-coplanar, i.e. $\Delta\Phi < 160^\circ$ ¹ complementary to the coplanarity condition. Further on, the neutron 4-momentum is reconstructed from the 4-momenta of proton and pion and it is checked, whether a calorimeter block in the corresponding (Θ, Φ) region recorded a hit without any additional entries recorded in the preceding detector elements of the Quirl. If these conditions are met, a neutron track is assumed. That way Θ_n and Φ_n are determined by the location of this calorimeter block. By this method we obtain a neutron detection efficiency of 36 %. Thus having only the neutron energy undetermined experimentally we end up with 3 kinematic overconstraints for this channel. Corresponding kinematic fits were applied.

The luminosity of the experiment was determined from the analysis of pp elastic scattering, see (I). All data have been efficiency corrected by MC simulations of the detector setup by using the CERN GEANT3 [2] detector simulation package, which accounts both for electromagnetic and hadronic interactions of the ejectiles with the detector materials.

¹ $\Delta\Phi$ is defined as the projection of the opening angle between two tracks onto the plane normal to the beam vector. That way we have always $\Delta\Phi \leq 180^\circ$.

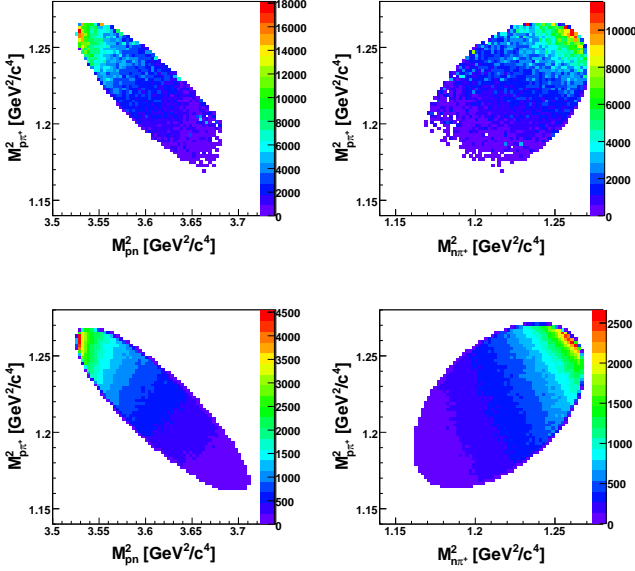


Fig. 1. Dalitz plots for the invariant mass combinations $M_{p\pi^+}^2$ versus M_{pn}^2 (left) and $M_{p\pi^+}^2$ versus $M_{n\pi^+}^2$ (right) as obtained for the $pp \rightarrow pn\pi^+$ reaction: on top for the data and on the bottom for the s-channel calculation (see text). Note that the plots for the data are efficiency but not acceptance corrected. The tiny deviations from the elliptic circumference at the upper corners are due to the excluded beam-hole region.

3 Results

Due to the identity of the collision partners in the entrance channel the angular distributions in the overall center-of-mass system have to be symmetric about 90° , i.e. the full information about the reaction channels is contained already in the interval $0^\circ \leq \Theta^{cm} \leq 90^\circ$. Deviations from this symmetry in the data indicate systematic uncertainties in the measurements. Hence we plot - where appropriate - the full angular range, in order to show the absence of major systematic errors in our measurement.

The total cross section of $0.47(2)$ mb for the $pp \rightarrow pn\pi^+$ reaction at $T_p = 400$ MeV is in good agreement with data at neighbouring energies [4, 5, 6, 7] – see next section and Fig. 5.

Differential distributions are shown in Figs. 1 - 4. Since a 3-body system in the final state has five independent variables, we choose to present the three invariant mass spectra M_{pn} , $M_{p\pi^+}$ and $M_{n\pi^+}$ as well as the proton and pion angular distributions in the overall center-of-mass system (cms). Because of the limited acceptance for pions only the angular range $0^\circ < \Theta_\pi^{cm} \leq 90^\circ$ is covered. However, as pointed out above, due to the 90° symmetry of the angular distributions yet the full information is contained in the data.

In contrast to the $pp\pi^0$ channel the Dalitz plots for the $pn\pi^+$ channel are far from being flat – see Fig.1. This is also borne out in the projections, the invariant mass spectra $M_{p\pi^+}$ and $M_{n\pi^+}$ (see Fig. 2, top), which peak just

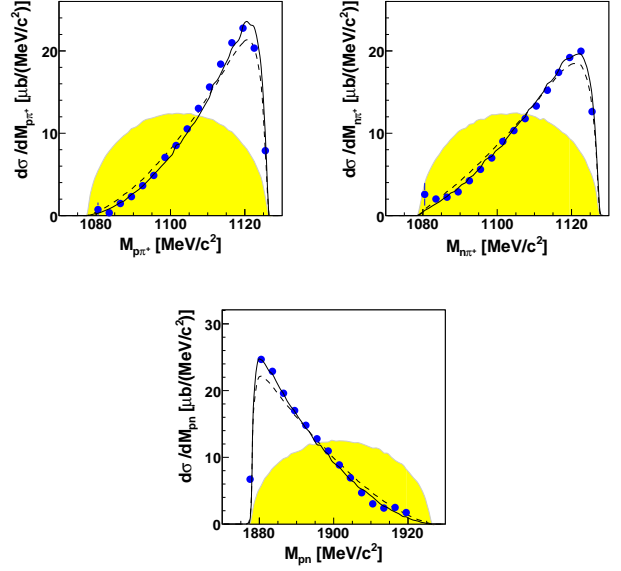


Fig. 2. Differential cross sections in dependence on invariant masses M_{pn} , $M_{p\pi^+}$ and $M_{n\pi^+}$ for the $pp \rightarrow pn\pi^+$ reaction. Data of this work are shown by full circles and phase space by the shaded area. Solid and dashed lines denote s-channel and t-channel calculations, respectively, as discussed in the text. For ease of comparison the calculations have been normalized to the experimental total cross section.

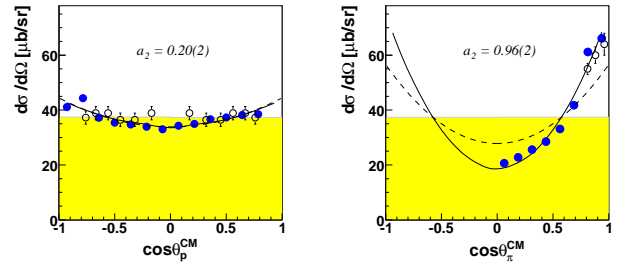


Fig. 3. Angular distributions of protons (left) and pions (right) in the center-of-mass system for the $pp \rightarrow pn\pi^+$ reaction. Data of this work are shown by full circles, WASA/PROMICE results [3] by open circles (renormalized to σ_{tot} of this work) and phase space by the shaded area. Solid and dashed lines denote s-channel and t-channel calculations, respectively, as discussed in the text. For ease of comparison the calculations have been normalized to the experimental total cross section. Given are also the Legendre coefficients a_2 from a Legendre fit according to eq. 2 in (I).

at the highest kinematical available masses. Complementary to these the M_{pn} spectrum (Fig. 2, bottom) peaks at lowest masses. Note that the high-mass enhancement is similar in both $M_{p\pi^+}$ and $M_{n\pi^+}$ spectra. This is in agreement with the trend observed in bubble chamber data at $T_p = 432$ MeV [8].

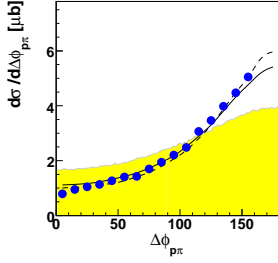


Fig. 4. Distribution of the planarity angle $\Delta\phi$ as defined in section 2 in the center-of-mass system for the $pp \rightarrow pn\pi^+$ reaction. Data of this work are shown by full circles and phase space by the shaded area. Solid and dashed lines denote s-channel and t-channel calculations, respectively, as discussed in the text. For ease of comparison the calculations have been normalized to the experimental total cross section.

Whereas the proton angular distribution is close to flat, the pion angular distribution is strongly anisotropic. It is fitted very well by a $(3\cos^2\Theta_{\pi^+}^{cm} + 1)$ distribution (solid line in Fig.3, right).

Our results are in good agreement with the results from PROMICE/WASA [3], which are the only other data available at $T_p \approx 400$ MeV. Note, however, that those measurements were carried out in a very limited phase space region only. E.g., in the PROMICE/WASA experiment the pion angular distribution was only measured for $\cos(\Theta_{\pi^+}^{cm}) \geq 0.79$.

By comparing the Dalitz plots from the data with those from the model calculations as shown in Fig.1 we see that we do not cover the full phase space in the experiment. However, we also see that the region not covered in these measurements is of very low cross section and hence contributes only marginally to the single-differential cross sections.

In Fig. 4 we show the spectrum of the planarity angle $\Delta\Phi$ defined and discussed in the previous chapter about the experiment. As pointed out there, we need the constraint $\Delta\Phi < 160^\circ$ in order to safely suppress $d\pi^+$ events. From Fig. 4 we see that this constraint does not cut away significant pieces of physics information. Any extrapolation into the cut region, be it by model or by phase space, will introduce uncertainties on the level of less than two percent.

4 Discussion of Results

For the comparison of $pn\pi^+$ and $pp\pi^0$ channels we show once more results in Figs. 6 and 7, which we obtained previously for the $pp\pi^0$ channel, see (I).

The proton angular distributions both in $pn\pi^+$ and $pp\pi^0$ channels are close to isotropic (see Figs. 3 and 7, left). They nevertheless show a tendency of opposite curvature, which just may be a reflection of the very different pion angular distributions in both channels. For the pion

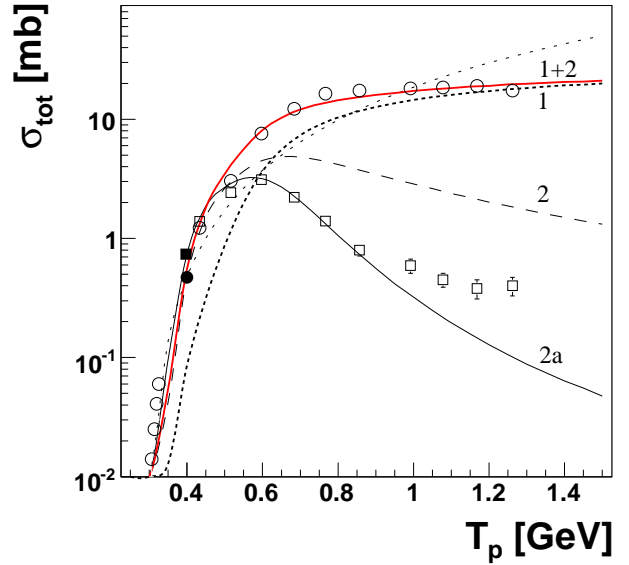


Fig. 5. Energy dependence of total cross sections for the reactions $pp \rightarrow d\pi^+$ (squares) and $pp \rightarrow pn\pi^+$ (circles). The filled symbols denote results of this work, open symbols are from [4, 5, 7]. Solid (2a) and dashed (2) lines represent s-channel calculations for $d\pi^+$ and $pn\pi^+$ channels, respectively, normalized to the data at $T_p = 400$ MeV. The t-channel calculation for the $pn\pi^+$ channel is given by the dotted lines (1) and normalized to the data at $T_p \geq 1$ GeV, where it is known to provide a reasonable description. The solid curve denoted by 1 + 2 is the sum of both processes for the $pp \rightarrow pn\pi^+$ channel. The short dashed curve indicates the energy dependence of the 3-body phase space.

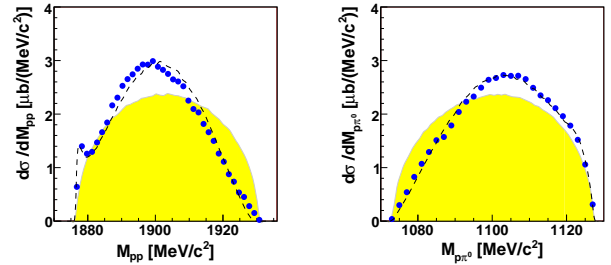


Fig. 6. Differential cross sections in dependence on invariant masses M_{pp} (left) and $M_{p\pi^0}$ (right) for the $pp \rightarrow pp\pi^0$ reaction (from (I)). Phase space is shown by the shaded area. For the explanation of the curves see (I).

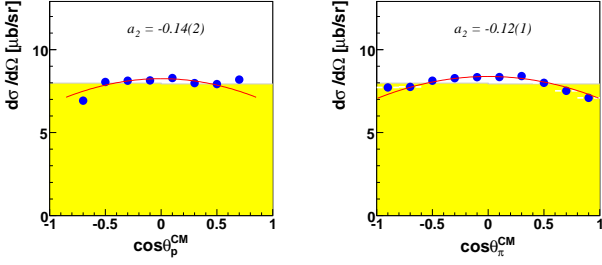


Fig. 7. Angular distributions of protons (left) and pions (right) in the center-of-mass system for the $pp \rightarrow pp\pi^0$ reaction (from (I)). The drawn curves represent Legendre fits, see (I).

angular distribution in case of $pp\pi^0$ we find a slightly concave shape (Fig. 7, right; Legendre coefficient $a_2 = -0.12$, see eq. 2 in (I)), whereas we get a strongly convex shape in case of the $pn\pi^+$ channel (Fig. 3, right; $a_2 = +0.96(2)$ with regard to eq. 2 in (I)).

A striking difference to the $pp\pi^0$ channel is the strong dominance of Δ excitation in the $pn\pi^+$ channel. In the $pp\pi^0$ channel Δ production in s-wave relative to the accompanying nucleon is prohibited by quantum numbers. However, as demonstrated in (I), the Δ production in relative p-wave is allowed and indeed contributes significantly to this channel already close to threshold.

The signature of Δ production in the $pn\pi^+$ channel is seen in all observables shown in Figs. 1 - 4. The M_{pn} spectrum (Fig. 2, bottom) is markedly different from the M_{pp} spectrum in the $pp\pi^0$ channel (Fig. 6, left). Though the pn final state interaction (FSI) is somewhat larger than the pp FSI, it cannot account for the huge difference between both spectra at low masses. It rather is a reflection from the complementary spectra $M_{p\pi^+}$ and $M_{n\pi^+}$, which peak just at the highest available masses (Fig. 2, top) in contrast to the $M_{pp\pi^0}$ spectrum observed in the $pp\pi^0$ channel (Fig. 6, right). This high-mass enhancement in turn has to be associated with Δ excitation.

The most striking feature in our $pn\pi^+$ data is the $(3 \cos^2 \Theta_{\pi^+}^{cm} + 1)$ dependence of the pion angular distribution. It is exactly this dependence, which is seen in πN scattering to the Δ resonance and which is also observed in the $pp \rightarrow d\pi^+$ reaction over a large range of incident energies. We note that also the pion angular distributions at $T_p = 420$ and 500 MeV, deduced from inclusive measurements of the $pp \rightarrow pn\pi^+$ reaction in Ref.[6] are basically in accord with this dependence.

We also note in passing, that in contrast to the situation in the $pp\pi^0$ channel, where we observe a strong dependence of the pion angular distribution on the relative momentum q between the two nucleons in the exit channel, we do not find such a behavior here. The pion angular distributions stay essentially the same for different q -regions. This again is in support of a single dominant mechanism proceeding via a single partial wave.

The close similarity in the angular distributions of $d\pi^+$ and $pn\pi^+$ channels is in agreement with the predictions

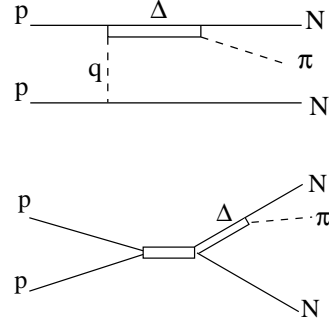


Fig. 8. Graphs used for the theoretical calculations. Top: t-channel approach (PWIA, direct part only), bottom: s-channel approach.

of Fäldt and Wilkin [9], according to which the meson angular distributions coincide closely in bound state and breakup channels near threshold.

The $(3 \cos^2 \Theta_{\pi^+}^{cm} + 1)$ dependence in the $pp \rightarrow d\pi^+$ reaction is due to the 1D_2 partial wave in the incident pp channel combined with the constraint of a p-wave pion relative to the deuteron in the exit channel. As known from phase shift analyses of this reaction [10,11] this 1D_2P partial wave dominates the $pp \rightarrow d\pi^+$ reaction basically from threshold up to $T_p \approx 900$ MeV. It is responsible for the resonance-like energy dependence of the total cross section and performs a perfect looping in the Argand diagram [10]. Thus this partial wave possesses all features to qualify for a s-channel resonance with $I(J^P) = 1(2^+)$ in the incident pp channel, the final $d\pi^+$ channel and the intermediate $N\Delta$ channel – see also discussion in Ref. [19]. From the total cross section of the 1D_2P partial wave in the $pp \rightarrow d\pi^+$ reaction [10] we see that the resonance energy is some 60 MeV below the nominal $N\Delta$ threshold, whereas the resonance width of ≈ 110 MeV corresponds to that of the Δ resonance.

The experimental observation that up to $T_p = 500$ MeV essentially a $(3 \cos^2 \Theta_{\pi^+}^{cm} + 1)$ dependence is observed also in the $pp \rightarrow pn\pi^+$ reaction points to the predominance of the 1D_2P partial wave in this reaction, too, as was already noted in Ref. [6]. From this also follows that the pn system at these energies is preferably in the deuteron-like quantum state $I(J^P) = 0(1^+)$.

The total cross sections for the single-pion production at $T_p = 400$ MeV have been presented and discussed already in detail in (I) [1]. For the $pp \rightarrow pp\pi^0$ and $pp \rightarrow d\pi^+$ channels our results are in good agreement with previous measurements. For the $pp \rightarrow pn\pi^+$ channel there are no experimental data to compare with at this particular energy. However, our result fits well to the trend given by the experimental results [4,5,6,7] at neighbouring energies – see also Fig. 5.

Finally we confront the data with simple theoretical calculations according to the graphs depicted in Fig. 8. First we start with a (properly antisymmetrized) t-channel approach in first-order impuls approximation, which is known to provide reasonable results for the angular distributions at energies $T_p \geq 1$ GeV [12,13,14,15,16]. For our

energy we show such a t-channel calculation by the dashed lines in Figs. 2 - 5. We see that the pion angular distribution is not reproduced correctly. The reason for this failure is simple. Since in this approach the Δ is excited by pion exchange between the two colliding nucleons, the reference axis for the pion decay of the excited Δ resonance is the momentum transfer q and not the beam axis. Note that the latter, however, is the reference axis for angles in the center-of-mass frame. Since the momentum transfer varies in dependence of the nucleon scattering angles, which are integrated over in the pion angular distribution, the calculated intrinsic $(3 \cos^2 \Theta_{\pi^+}^q + 1)$ dependence in the t-channel approach appears to be smeared out in the cms pion angular distribution.

In order to establish the beam direction as the appropriate reference axis for the pion angular distribution in the calculation one either has to reiterate the pion exchanges and sum them up to infinity or simply make a s-channel ansatz. The latter is easily made by a Breit-Wigner ansatz for the 1D_2 resonance (Fig. 8, bottom), which dissociates into a $N\Delta$ system in relative s-wave followed by the decay of the Δ resonance. This grants the observed $(3 \cos^2 \Theta_{\pi^+}^{cm} + 1)$ dependence for the pions as well as the desired shape of the invariant mass spectra. To simulate the $pp \rightarrow d\pi^+$ reaction within this ansatz we impose the Hulthen wave function as condition for the Fermi momentum between proton and neutron. For the $pp \rightarrow pn\pi^+$ reaction we impose a FSI interaction of Migdal-Watson type [17,18] on the pn system. These calculations are shown by the Dalitz plots in Fig. 1, bottom and by the solid lines in Figs. 2 - 5. They give a good account of the differential distributions both for the invariant masses and for the particle emission angles.

Mass (2.07 GeV) and width (80 MeV) of the $I(J^P) = 1(2^+)$ resonance in this s-channel ansatz have been chosen to reproduce the energy dependence of the total cross section of the $pp \rightarrow d\pi^+$ reaction in the region of the 1D_2P dominance, i.e. up to $T_p \approx 700$ MeV. That way we simultaneously get a good description for the energy dependence of the total cross section for the $pp \rightarrow pn\pi^+$ reaction up to $T_p \approx 600$ MeV. If combined with the amplitude of the t-channel approach we even obtain a reasonable description of the total cross sections up to the GeV region (Fig. 5).

5 Summary

We have presented measurements of the $pp \rightarrow pn\pi^+$ reaction at $T_p \approx 400$ MeV. In this energy region they are the first exclusive ones of solid statistics to cover most of the reaction phase space. The differential distributions are characterized by the overwhelming dominance of the Δ excitation. The pion angular distribution coincides with that observed in the $pp \rightarrow d\pi^+$ channel, which in turn is dominated by the resonating 1D_2P partial wave. From this coincidence we conclude that also the $pn\pi^+$ channel is dominated by the same s-channel resonance in the near-threshold region. The correlation between boundstate and breakup channels is in accordance with the predictions by Fäldt and Wilkin [9].

This work has been supported by BMBF, DFG (Europ. Graduiertenkolleg 683) and COSY-FFE. We acknowledge valuable discussions with R. A. Arndt, L. Alvarez-Ruso, D. Bugg, C. Hanhart, M. Kaskulov, V. Kukulín, E. Oset, I. Strakovsky, W. Weise and C. Wilkin.

References

1. S. Abd El-Samad et al., Eur. Phys. J. **A30**, 443 (2006)
2. CERN Computing and Networks Division, *GEANT - Detector description and Simulation Tool*, CERN Program Library
3. A. Betsch et al., Phys. Lett. **B446**, 179 (1999)
4. for a data compilation see J. Bystricky et al., J. Physique **48**, 1901 (1987)
5. F. Shimizu et al., Nucl. Phys. **A386**, 571 (1982)
6. R. G. Pleydon et al., Phys. Rev. **C59**, 3208 (1999)
7. J. G. Hardie et al., Phys. Rev. **C56**, 20 (1997)
8. F. Shimizu et al., Nucl. Phys. **A389**, 445 (1982)
9. G. Fäldt and C. Wilkin, Phys. Lett. **B382**, 209 (1996) and **B389**, 440 (1996)
10. R. A. Arndt et al., Phys. Rev. **C48**, 1926 (1993); SAID data base see also <http://said.phys.vt.edu>
11. R. A. Arndt, Phys. Rev. **165**, 1834 (1968)
12. V. Dmitriev, O. Sushkov, C. Gaarde, Nucl. Phys. **A459**, 503 (1986)
13. S. Huber, J. Aichelin, Nucl. Phys. **A573**, 587 (1994)
14. P. Fernandez et al., Nucl. Phys. **A586**, 586 (1995)
15. S. Teis et al., Z. Phys. **A356**, 421 (1997)
16. V. Sarantsev et al., Eur. Phys. J. **A21**, 303 (2004)
17. A. B. Migdal, J. Exp. Theor. Phys. **28**, 1 (1955)
18. K. W. Watson, Phys. Rev. **88**, 163 (1952)
19. H. Clement et al., Prog. Part. Nucl. Phys. **61**, 276 (2008); arXiv: 0712.4125 [nucl-ex]